ACS APPLIED MATERIALS & INTERFACES

Research Article

www.acsami.org

Vertical Arrays of SiO_2 Micro/Nanotubes Templated from Si Pillars by Chemical Oxidation for High Loading Capacity Buoyant Aquatic Devices

Sung-Soo Yoon and Dahl-Young Khang*

Department of Materials Science and Engineering, Yonsei University, Seoul 120-749, Korea

Supporting Information

ABSTRACT: A simple and facile method to fabricate SiO_2 micro- or nanotubes has been demonstrated based on room temperature wet chemical oxidation of a porous layer of Si pillar templates that have been prepared by metal-assisted chemical etching (MaCE). Under typical conditions, Si pillars produced by the MaCE have been found to be covered with a thin nanoporous Si layer. The porous Si skin layer has been chemically oxidized by simple dipping in $AgNO_3$ solution at room temperature, which has led to seamless SiO_2 shell layer thanks to the accompanying volume expansion during the wet oxidation. Following wet removal of core Si by KOH yields the SiO_2 micro- or nanotubes, either in test tube shape or in open shape at both ends, depending on processing method. The vertical arrays of the SiO_2 tube on the Si substrate, after hydrophobic siloxane oligomer printing, has been found to have very large loading capacity on water, due to extremely high porosity (>90%) and good enough mechanical stability. The novel method to fabricate SiO_2 tubes can shed new light in design of novel aquatic devices, other than simple mimicking the leg of a water strider. Also, the method may be very helpful in various applications of SiO_2 nanotubes.

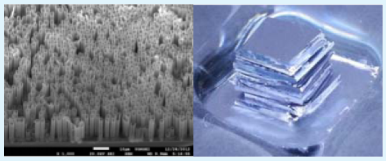

KEYWORDS: *Si pillar, SiO_2 nanotube, porous Si, chemical oxidation, aquatic devices*

1. INTRODUCTION

Silica (SiO_2) micro- and nanotubes have been actively studied for various envisioned applications, ranging from gene/drug delivery, bioseparation and catalysis to hydrogen storage.[1−3] In addition to its intrinsic hydrophilic nature, it can be easily functionalized on its surfaces (inner and/or outer) for a specific application, which makes its dispersion in various solvents feasible at the same time.[2] Accordingly, various approaches for the synthesis/fabrication of SiO_2 nanotubes have been proposed in literature. Using proper templates, such as anodic aluminum oxide (AAO),[2] nanowires[4] and multiwalled carbon nanotubes,[5] bio templates,[6] and self-assembled nanostructures of amphiphiles,[7] SiO_2 nanotubes have been shown to be successfully prepared. In these template-based approaches, synthetic approaches such as sol−gel, hydrothermal, and microemulsion, have been applied for the preparation of SiO_2 tubes on/in the templates. Direct deposition, such as atomic layer deposition (ALD), of materials onto such templates has also been demonstrated to obtain interesting coaxial multiwalled nanotubes.[8] Furthermore, a Si nanowire arrays template has been successfully converted into SiO_2 tube ones by applying semiconductor processing techniques such as high temperature oxidation followed by plasma etching to selectively remove the core Si.[9]

In the present work, we demonstrate a simple method for the facile preparation of SiO_2 micro-/nanotubes from the Si pillar template. The vertical arrays of Si pillars were prepared by the well-known metal-assisted chemical etching (MaCE) method,[10−12] in combination with colloidal monolayer mask. Compared to bottom-up methods, vapor-liquid-solid (VLS) growth for example,[13] the MaCE of Si is very easy and simple: it can be carried out by wet chemical etching with suitable noble metal catalysts such as Pt, Au, or Ag, thus avoiding the use of expensive equipment/process and vacuum. Recent studies have also shown that the Si micro-/nanopillars fabricated by the MaCE have a very rough surface, or porous surface layer.[14−17] In general, the porous layer should be avoided, though the rough or porous skin layer on Si pillars may be useful in certain applications.[18] In this work, the porous skin layer was advantageously utilized for wet chemical oxidation of Si at room temperature. Contrary to the conventional high temperature thermal oxidation, the wet chemical oxidation can be carried out at room temperature by simple dipping in an oxidizing solution.[19,20] Interestingly, the room-temperature chemical oxidation has resulted in a dense and mechanically robust SiO_2 layer with very few defects, in spite of the porous nature of the starting material.

The SiO_2−Si core−shell pillars formed by the wet chemical oxidation can be successfully turned into SiO_2 tubes by the etch removal of the core Si with KOH solution. The SiO_2 tube dimensions, such as diameter and length, can be easily controlled by using Si pillars prepared at different MaCE conditions. Furthermore, the vertical arrays of SiO_2 tube on Si substrate have been found to have a very high loading capacity on water after hydrophobic surface treatment by contact-printing of siloxane oligomers,[21,22] which may be very useful in

Received: October 4, 2013
Accepted: December 6, 2013
Published: December 6, 2013

 © 2013 American Chemical Society dx.doi.org/10.1021/am4043504 | ACS Appl. Mater. Interfaces 2013, 5, 13441−13447

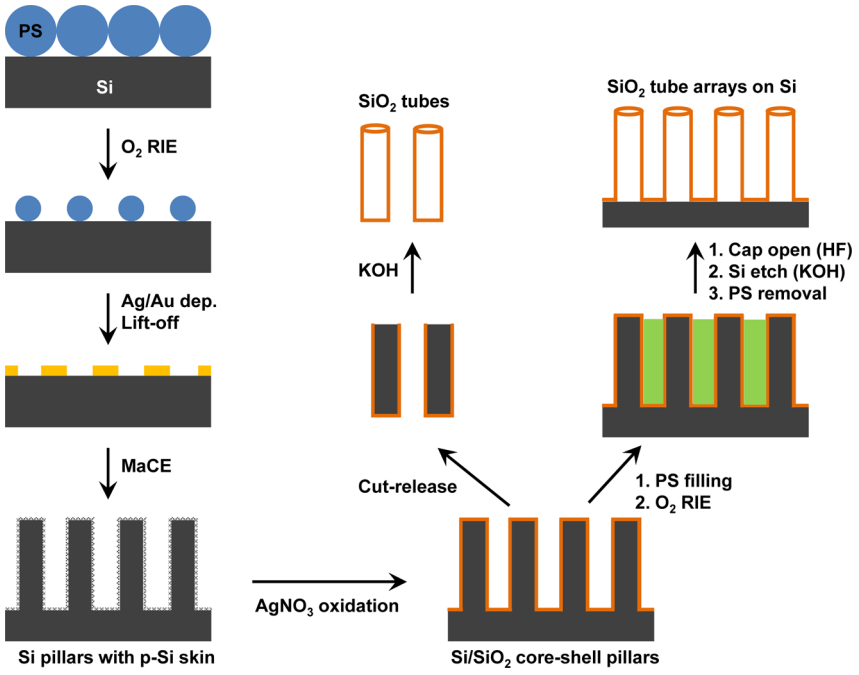

Figure 1. Schematic drawing of the fabrication steps for SiO_2 micro-/nanotubes from vertical Si pillar array template.

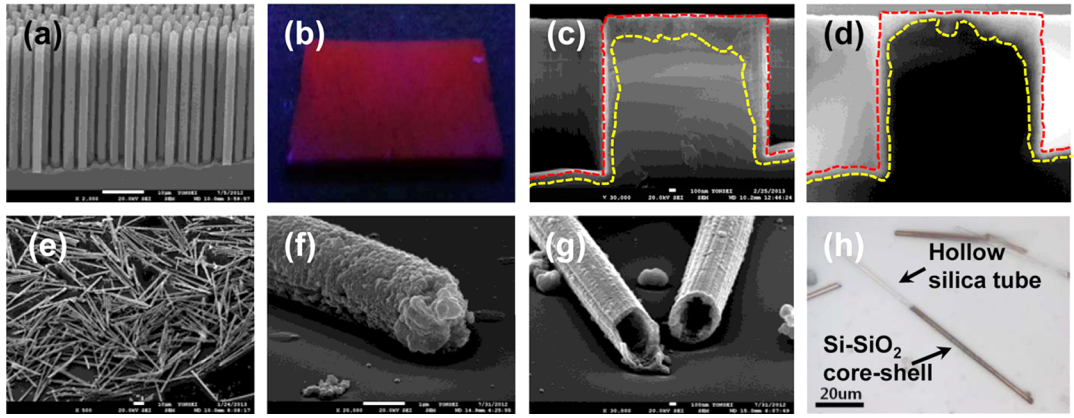

Figure 2. (a) SEM image of vertical Si pillar (~2 μm in diameter and ~35 μm long) arrays fabricated by metal-assisted chemical etching of Si. (b) Photograph of red-luminescent Si pillars due to the porous Si skin layer (excited by 254 nm UV light). (c, d) SEM images of Si pillars, secondary electron (SE) mode (c) and backscattered electron (BSE) mode (d), respectively. Red lines delineate the contour of pillars whereas yellow ones designate the boundary between p-Si and the solid Si core, respectively. (e) SEM image of released SiO_2 tubes templated from Si pillar arrays shown in panel a. (f, g) High magnification SEM images of the closed end (f) and the open end (g), respectively, of SiO_2 tubes. (h) Optical microscope (OM) image of released Si pillars after incomplete KOH etching of core Si. The transparent portion denotes the hollow SiO_2 tube, whereas the colored one is the Si-SiO_2 core−shell pillar.

developing novel aquatic devices. The extreme porosity (>90%) of the SiO_2 tube arrays structure, with excellent mechanical integrity at the same time, has been found to be a key element for such a high loading capacity. The observed high loading capacity of SiO_2 tube arrays can shed new light on the design of water-buoyant devices, beyond the simple bio-mimicking of a leg of a water strider.[23−28]

2. RESULTS AND DISCUSSION

Si pillar arrays were prepared by the MaCE in H_2O_2/HF solution with a patterned Au(20 nm)/Ag(30 nm) bilayer metal film as a catalyst.[29] The metal mesh film was fabricated by polystyrene (PS) colloidal monolayer formation, size reduction with O_2 reactive ion etching (RIE), metal deposition, followed by lift-off of colloidal spheres, as shown in Figure 1. The diameter of the resulting Si pillar arrays is primarily determined by the size of PS colloids used and the time duration of the O_2 RIE step. In this work, PS colloids of ~3.1 μm and ~600 nm were used, and the resulting Si pillar diameters were found to be ~2 μm and ~500 nm, respectively. The length of the Si pillar arrays could be easily controlled by simply changing the MaCE time. As is now well-known, the MaCE process leads to the formation of a thin p-Si skin layer on exposed Si surfaces.[14−17] The p-Si layer was found to be mostly nanoporous, which means the pore size is in the range of <~10 nm. After a simple dip in a $AgNO_3$ solution at room temperature, the p-Si layer was oxidized into SiO_2.[19,20] At this stage, the Si pillar arrays are now a Si/SiO_2 core−shell geometry, to be exact. After those core−shell pillars were released off the substrate by razor blade, the core Si was further

etched away by KOH, leading to the formation of hollow SiO_2 tubes. Or, in a slightly different scheme shown in the right-most part of Figure 1, the vertical arrays of a Si/SiO_2 core−shell pillar on Si substrate was filled with polystyrene (PS) first by spin-coating. Then O_2 RIE was applied to reveal the top portion of the pillars and was exposed to dilute HF solution briefly to remove the oxide cap on top of the pillars. The core Si was removed by KOH. Final dissolution of the embedded PS layer with toluene has resulted in the vertical arrays of SiO_2 tube on the Si substrate.

Figure 2a shows the scanning electron microscope (SEM) image of vertical Si pillar arrays (more data on Si pillars and the corresponding SiO_2 tubes differing in diameter and length, or aspect ratio, can be found in the Supporting Information, Figure S1). The existence of the p-Si skin layer on the exposed Si surfaces after the MaCE step can be easily confirmed by light emission under UV excitation. Figure 2b shows the photograph of the Si pillar arrays sample right after the MaCE and cleaning, under the UV (254 nm) excitation. As is well-known in p-Si literature,[30] the red color is the evidence for the existence of nanoporous Si. Also, the p-Si layer on the pillar surface can be identified under the secondary electron (SE) mode SEM imaging as shown in Figure 2c, though the contrast between the porous skin layer and the nonporous, solid Si core is not quite good. On the other hand, the enhanced contrast in back-scattered electron (BSE) mode SEM imaging shows clearly the existence of a nanoporous skin layer on Si pillars, as shown in Figure 2d. In Figure 2c,d, dotted lines in red show the contour of a Si pillar, whereas yellow ones delineate roughly the boundary between nanoporous and solid Si, respectively.

Figure 2e−g shows the fabricated SiO_2 tubes by the method developed in this work. As shown in Figure 2f,g, the tubes show a rather rough inner and outer surface, which is reminiscent of nanoscale nonuniformity in the MaCE and p-Si layer formation (Supporting Information, Figure S2, where TEM images show the detailed inner structure of the tubes). Note here that the tubes are a kind of "nano/micro test tube"; in other words, one end of the tubes is closed while the other end is open (Supporting Information, Figure S3). This test tube structure would be very beneficial for various applications such as, for example, drug delivery. Furthermore, the dimensions of the SiO_2 tubes, such as diameter and length, can be varied by controlling those of the starting Si pillars (Supporting Information, Figure S1) up to a tube aspect ratio of ∼100. If the KOH etching for the removal of Si core is incomplete, the final structure is the partly hollow tube and partly core−shell pillars, as shown in Figure 2h. This "hybrid" nanostructure can easily be observed under an optical microscope, due to different optical transparencies between the hollow, transparent SiO_2 tube portion and the opaque core−shell one.

Using another process scheme, the tube arrays can be formed on the mother Si substrate, i.e., vertical SiO_2 tube arrays on Si, as shown in Figure 3a. It should be noted that the nonpillared surface of the Si substrate became porous too, as can be seen in Figure 1c,d, and thus oxidized during $AgNO_3$ dip. Therefore, the whole arrays of SiO_2 tubes can be lifted off the substrate, if the KOH etching is done for a sufficiently long time: KOH will etch-remove Si not only underneath the pillars but also under the nonpillared area. Then the whole arrays of SiO_2 tubes can be picked up onto an elastomeric polydimethylsiloxane (PDMS) substrate, as shown in Figure 3b. The end of tubes picked onto PDMS show a noncircular shape, due to concurrent detachment of the oxide layer formed on the

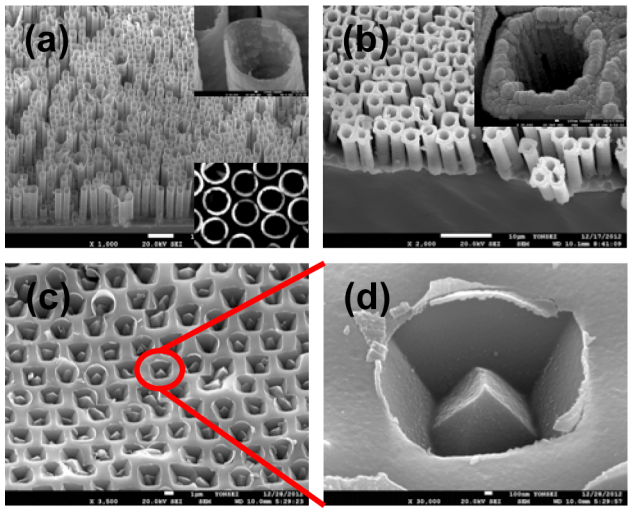

Figure 3. (a) SEM images of vertical arrays of hollow SiO_2 tubes on Si substrate. (Insets) magnified images of the tube arrays, tilted (upper right) and top (lower right) views, respectively. (b) SiO_2 tube arrays that are partially embedded in elastomeric polydimethylsiloxane (PDMS) substrate, with a zoomed view as the inset. (c, d) Si substrate after removal of vertical SiO_2 tube arrays by razor blade. The central part of each hole contains a pyramid, which is reminiscent of anisotropic etching of Si by KOH. Note also the thin and continuous crustlike layer of SiO_2 around the holes.

nonpillared area. It should be noted that the tubes in this process scheme are open at both ends, contrary to tubes shown in Figure 2, which might be very useful for materials delivery to living cells using such a "nanoneedle" array.[31] The SEM images of the remaining Si surface again confirms the existence of a thin oxide crust layer on the nonpillared surface, as shown in Figure 3c,d. Also, the central part of each hole contains a pyramid, which is a reminiscent of anisotropic etching of Si by KOH.

To elucidate and confirm the wet chemical conversion of p-Si into SiO_2 by dipping in $AgNO_3$, the sample was imaged by SEM right after the $AgNO_3$ oxidation step, as shown in Figure 4a. The exposed Si surface, including the outer surface of the Si pillars and the areas between the pillars, were found to be covered with Ag particulates, ranging from tens of nanometers to micrometers (Supporting Information, Figure S4; also Figure S4 contains elemental analysis by EDX on Si pillars, before/after oxidation and after oxide strip). The Ag ions in $AgNO_3$ solution are reduced and nucleated into particles by taking electrons from the exposed Si surface, while the Si is oxidized into SiO_2 at the same time, i.e., electrochemical redox reactions given as

$$Ag^+ + e^- \rightarrow Ag \quad (1)$$

$$Si + 2H_2O \rightarrow SiO_2 + 4H^+ + 4e^- \quad (2)$$

Notably, most of the SiO_2 tubes showed dense and continuous tube wall, in spite of the nanoporous nature of the pillar surface that is oxidized. This is due to volume expansion during the oxidation of Si into SiO_2, as is well-known in the Si industry.[32] However, pinholes and small openings on tube walls were spottedly observed, as shown in Figure 4b. The mechanical integrity of the tube wall is primarily determined by the initial microstructure of p-Si to be oxidized. The defects such as holes can occur when the p-Si skin layer has rather large pores, larger than certain critical size that exceeds the degree of

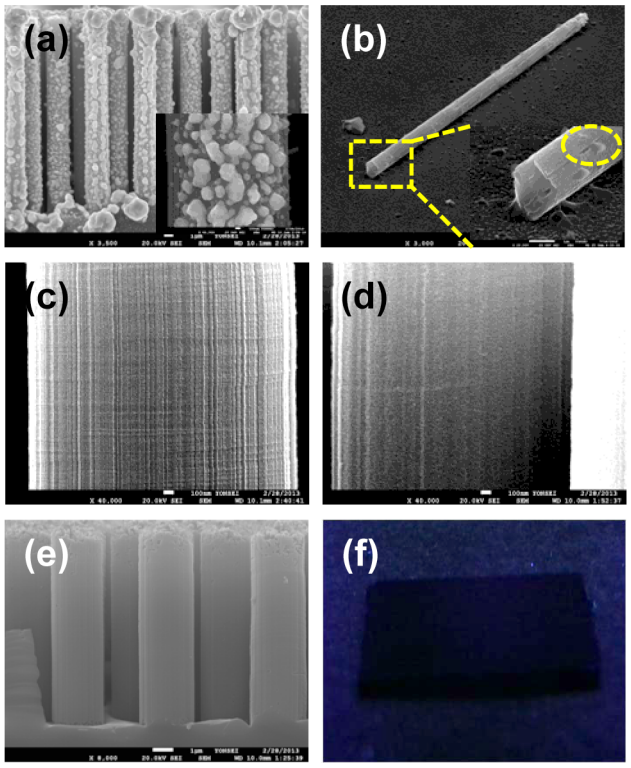

Figure 4. (a) Cross-sectional SEM image of a Si pillar sample right after the wet chemical oxidation in $AgNO_3$ solution. The Ag ions are nucleated into particles on the outer surface of pillars during the wet oxidation. (b) SiO_2 tube with a defective hole on its sidewall. (c, d) Comparison of surface morphology of a Si pillar: as-prepared (c) and after the wet oxidation (d), respectively. Note here that the pillar surface becomes smoother after the wet oxidation, which indirectly means that the formation of a SiO_2 layer accompanies the volume expansion during the wet oxidation. (e) Vertical arrays of a solid Si pillar, after removing the porous Si skin layer by wet oxidation and HF strip. (f) Photograph of solid Si pillar arrays under UV illumination, showing no light emission due to the absence of a porous Si layer.

volume expansion during wet chemical oxidation. We believe that those defects can be minimized (or even eliminated completely) by optimizing the MaCE in terms of p-Si formation as well as pillar geometry.

Another experimental evidence on the volume expansion during the wet chemical oxidation of p-Si is the smoothening of pillar surface after the oxidation, as shown in Figure 4c,d. Before oxidation (right after the MaCE and cleaning), the pillar surface has numerous vertical and horizontal striations, due to nonuniform etching during MaCE at the nanoscale. Those striations, especially horizontal ones, almost completely disappeared after the wet oxidation. As shown in Figure S2 (Supporting Information), the pillar surface returns back to the striated state by an oxide strip with HF. Finally, the approach can be exploited to make a nonporous, solid Si pillar array: the porous skin layer can be completely removed by the wet oxidation in $AgNO_3$ and following a HF strip, as shown in Figure 4e,f. The solid Si pillar arrays show no light emission under UV illumination (compare this with the clear red photoluminescence from p-Si pillars shown in Figure 2b). It seems that the p-Si skin always forms in Si pillars prepared by MaCE, regardless of processing conditions such as substrate doping type, etchant formulation, etc.[14−17] Although the p-Si skin formation can be avoided (or minimized) by optimizing MaCE conditions, the present method be a quick and simple way to prepare solid Si pillar arrays.[14]

Finally, the SiO_2 tube arrays on Si substrate have been applied as a load-bearing aquatic device, which mimics the well-known water strider legs.[23−28] To make the surface in contact with water hydrophobic, simple contact-printing of siloxane oligomers that diffuse out of a cured PDMS stamp was used (typical fluorinated self-assembled monolayer (F-SAM) showed the same results, though data are not shown here).[21,22] The water contact angles (CA) on siloxane-printed Si pillar and SiO_2 tube arrays are shown in Figure 5a. Due to surface roughness endowed by microstructuring of pillar/tube geometries, those surfaces became superhydrophobic, i.e., water CA exceeds 150°. Also, the CA value does not show any noticeable difference between pillar and tube arrays.

The maximum loading capacity, the weight supported by the sample of unit area just before sinking down into water bath, was measured by adding weight onto the back-surface of samples floating on water, as shown in Figure 5b. Both the Si pillar and SiO_2 tube samples showed a decent loading capacity, not sinking into water under an applied load. Rather, the samples form deep dimples, as can be seen in the photographs. The measured maximum loading capacity of various samples is plotted in Figure 5a. Interestingly, the tube sample showed much higher loading capacity than the Si pillar one: a ∼10 μm long SiO_2 tube has similar loading capacity to a ∼20 μm long pillar sample. Further, the loading capacity increases almost linearly as the tube length increases from ∼10 μm to ∼40 μm, then seems to saturate at ∼0.8 g/cm^2 upon further increase of tube length. The maximum loading capacity of ∼0.8 g/cm^2 obtained with SiO_2 tube arrays in this work is the best value, to the best of authors' knowledge (cf. ∼0.5 g/cm^2 in ref 26.). Also, the use of hollow superhydrophobic structure, as superhydrophobic SiO_2 tube arrays demonstrated in this work, can lead to new direction for the fabrication of biomimetic aquatic devices having high loading capacity.

First, the high loading capacity of Si pillar and SiO_2 tube arrays is due to the formation of an air sheath around the sample surface when the sample is made in contact with water, or the so-called plastron effect.[28,33] As can be seen in the bottom panel of Figure 5c, the siloxane-printed superhydrophobic surfaces of Si pillars and SiO_2 tubes show silvery sheen in water due to the existence of the air sheath. On the other hand, hydrophilic surfaces do not show such glisten (top panel, Figure 5c). The hydrophilic Si pillar surface looks dark brown in water, whereas the superhydrophobic Si pillar surface shows silvery glisten. In the case of SiO_2 tube samples, the difference is not so distinct as in the case of Si pillar samples.

The reason for the much higher loading capacity of SiO_2 tube sample than that of Si pillar one can be explained based on the larger buoyant force for the tube sample. The extra buoyant force (ΔF_b) that is achieved by including air void in immersed sample volume can be written as[34,35]

$$\Delta F_b = \rho_w V_{air} g \propto \varepsilon \tag{3}$$

where the ρ_w, V_{air} and g denote the density of water, air volume, and gravitational constant, respectively. The volume of air can also be expressed as the product of porosity and total volume, resulting in the last expression. The fraction of void, or porosity (ε), can be roughly estimated by simple geometric consideration, i.e., nonclose packed hexagonal array, as given in Figure 5d. For the Si pillar sample, the calculated porosity is ∼60% by assuming s ∼ 1.5 d and d ∼ 2 μm (s, center-to-center distance;

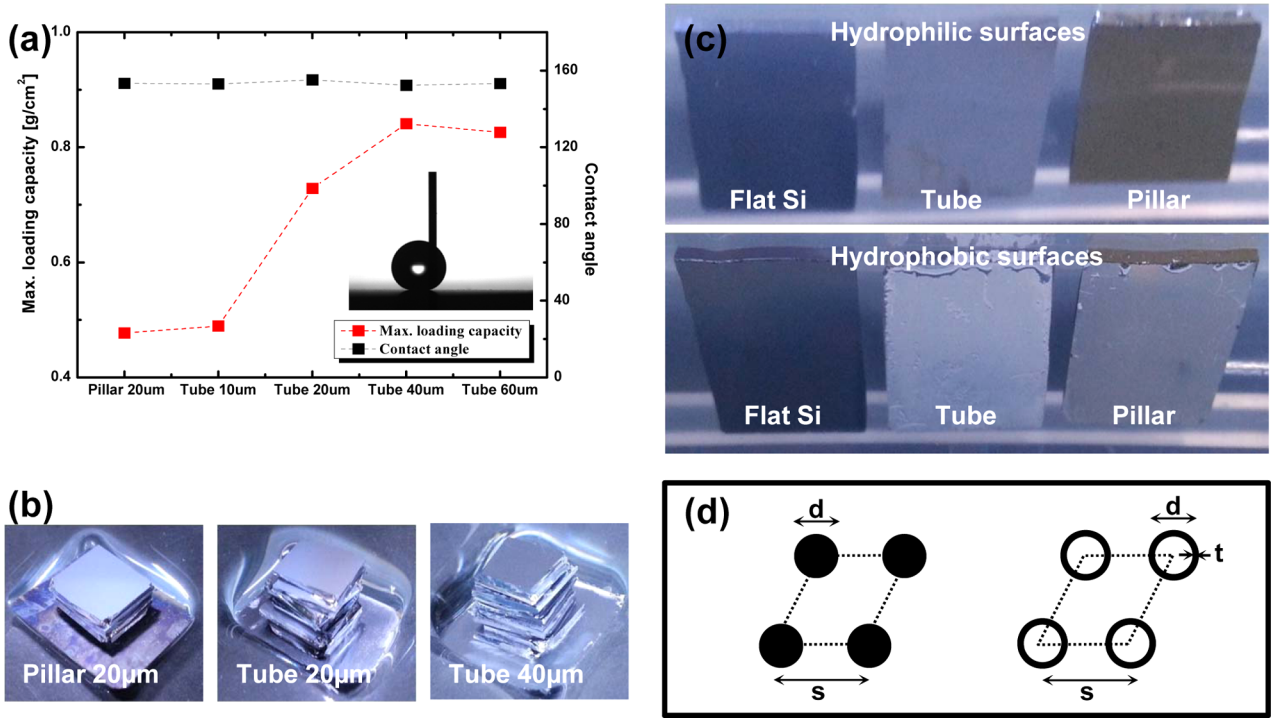

Figure 5. SiO_2 tube arrays as high loading capacity aquatic devices. (a) Contact angle and maximum loading capacity of Si pillar and SiO_2 tube arrays, as a function of length. (b) Digital photographs of samples floating on water under loading. (c) Photographs of samples immersed in water: air-sheath (or, "plastron") can be seen in hydrophobized surfaces. (d) Simplified drawings for porosity calculation of Si pillar (left) and SiO_2 tube (right) arrays.

d, pillar diameter). On the other hand, the porosity reaches up to ~92% for SiO_2 tube arrays, with a tube thickness value of 0.1 μm (Supporting Information, Figure S3). Therefore, the calculated air volume for ~20 μm long Si pillar arrays sample yields to similar value obtained from ~10μm long SiO_2 tube arrays sample, leading to a similar loading capacity, as shown in Figure 5a. In other words, the extremely high porosity (>90%) of SiO_2 tube sample enables the large buoyant force and thus the very high loading capacity, much higher than its pillar counterpart.

Although those high aspect ratio structures, both Si pillars and SiO_2 tubes, seem to be prone to lateral collapse during sample preparation or upon repeated tests on water for loading capacity measurements,[36,37] they showed strong enough mechanical stability, leading to no obvious lateral collapse or breakage. This is due to the fact that the samples have a densely populated regular array of micro/nano structures, counter-balancing capillary forces acting during drying after wet processes. Also, the samples in the loading test on water are in normal stress, rather than in shear mode; furthermore, they are not in direct contact with water due to the presence of air sheath. Therefore, those samples have enough mechanical strength even with such high (60%−90%) porosity. It should be noted that such a high porosity value (>90%) can be obtained by conventional porosification of Si,[30] but the resulting structure is very fragile and thus prone to collapse during drying due to very high capillary force, unless special steps are taken such as super-critical drying.

The linear increase in the maximum loading capacity of SiO_2 tube samples with the increase of tube length, from ~10 μm up to 40 μm, can be explained by eq 3, too. Although the porosity of tube sample remains the same regardless of tube length, the absolute volume of air contained in the structures increases linearly with the tube length. This linear increase in the volume of air results in the observed linear increase in loading capacity. However, the loading capacity saturates at tube lengths of >~40μm. The observed saturation behavior is due to the flooding of water dimple onto the backside of sample, as shown in Figure S5 (Supporting Information). The meniscus of water, or the dimple shape, remains the same as the shape of the sample up to the maximum loading capacity. Above the maximum loading capacity, however, the water dimple starts to flood over the back surface of the sample, forming symmetric circular meniscus, and finally leading to sink down of the sample. Considering the fact that the edges and back-surface of samples did not have any special treatment, we infer that the delay of such flooding and thus increase in loading capacity may be possible with further treatment on the sample perimeters and back-surface.

3. CONCLUSION

Mechanically robust SiO_2 micro/nano tubes have been successfully fabricated using the Si pillar template. The porous layer on Si pillar after MaCE has been converted into SiO_2 by wet chemical oxidation at room temperature, i.e., simple dipping in $AgNO_3$ solution. Thanks to the volume expansion accompanying the chemical conversion, the initial porous structure became seamless tube wall with few defective holes. Removal of the core Si by KOH etching has led to SiO_2 tubes, either dispersed on a substrate or in a vertical array form on mother Si substrate depending on the process scheme used. Interestingly, the vertical arrays of a hydrophobized SiO_2 tube on Si have been demonstrated as a very high loading capacity aquatic device on water. The key element of the observed high loading capacity of the SiO_2 tube structure has been found to have high porosity, >90%, while still maintaining good

mechanical robustness. This may open a new direction in the field of biomimetic aquatic devices.

4. EXPERIMENTAL SECTION

4.1. Colloidal Monolayer Formation. A Si(100) wafer was cut into small pieces (~1.5 cm × 3 cm) and cleaned by sequential baths of acetone, isopropyl alcohol, and deionized (DI) water, with ultrasonication. The colloidal PS particles (3.1μm or 600 nm, Bead and micro) dispersed in DI water at 2 wt % was slowly applied on a still water surface. Then, 2% surfactant solution (Sodium Dodecyl Sulfate, Aldrich) diluted in DI water was dropped onto one corner of the water bath containing PS particles. The formation of surfactant monolayer on free surface plays the role of compression barrier, like a mechanical barrier in conventional Langmuir-Blodgett trough, leading to compaction of floating PS particles into a close-packed hexagonal monolayer. Cleaned Si substrate was used to lift-up the formed PS monolayer in the bath. The PS/Si sample was further treated with O_2 reactive ion etching (RIE; Japan Pionics, WGC-20B-1-S) to reduce the size of PS particles, while maintaining the hexagonal arrangement.

4.2. Metal-Assisted Chemical Etching of Si. A bilayer metal catalyst of Au(20 nm)/Ag(30 nm) was deposited on the PS/Si substrate by e-beam evaporation. Following with lift-off of the PS particles led to a catalytic metal mesh pattern on the Si substrate. Then the MaCE was done in an etching solution of H_2O_2 (0.045M), HF (0.5M), and DI. During the MaCE, the metal mesh film drilled down into the Si substrate, forming a Si pillar structure of an unetched portion of Si. It is noted that the dimensions (diameter and length) of Si pillar are mainly determined by the PS size after the O_2 RIE and etching duration, respectively. For the wet chemical oxidation, the Si pillar arrays sample was simply dipped into 0.1M $AgNO_3$ solution, typically for 4 h, at room temperature. The oxide thickness is determined by the thickness of porous Si layer formed during the MaCE step. After removal of Ag particle by HNO_3, the Si/SiO_2 core−shell pillars were released by razor blade. Removal of core Si by KOH solution did finally lead to micro/nano test tubes, in that one end of the tubes is closed while the other end is open. A slightly different scheme was used to fabricate vertical arrays of SiO_2 tubes on the Si substrate. Instead of release-cut of the Si/SiO_2 core−shell pillars, a sacrificial layer of polystyrene was filled into the voids between the pillars by spin-coating. Then the excess layer of PS covering the top portion of the pillars was etched by O_2 RIE to reveal the pillar top. Brief exposure to a solution of diluted HF removed the oxide cap at the end of the pillars. KOH etching of core Si and toluene washing of the embedding PS finally led to the vertical arrays of SiO_2 tube on the Si substrate.

4.3. Buoyant Aquatic Devices. The vertical arrays of a SiO_2 tube on Si substrate was made hydrophobic by contact-printing of siloxane oligomers. For this, a cured slab of PDMS (Sylgard 184, Dow) was simply made in contact with the top surface of a SiO_2 tube sample for overnight, which lead to hydrophobic printing by diffused-out, uncured siloxane oligomers. Then the sample was flipped over and floated onto a water bath. Note here that the Si substrate plays the role of mechanical support to ensure the SiO_2 tubes stay upright upon facing the water surface. Small pieces of Si wafers were added onto the sample as a load to measure the loading capacity.

4.4. Characterizations. Optical microscope (Olympus, BX51) and scanning electron microscope (Jeol, JSM6700F) were used to image the sample. Water contact angle on Si pillar and SiO_2 tube surfaces was measured by optical tensiometer (Attention, Theta). The photoluminescence from the porous Si skin layer on a Si pillar was measured by using an UV lamp (Uvitec, LF-206.LS) with an excitation wavelength of 365 nm.

■ ASSOCIATED CONTENT

Ⓢ Supporting Information

SEM images of vertical arry of Si pillar and corresponding silica tubes with different diameter and length. SEM images of surface morphology of Si pillar at different stages of processing and TEM images for detailed structure analysis of tubes inside. SEM images of closed-end and open-end of silica nano tubes. SEM images of Si pillar sample with nucleated Ag particles after the wet oxidation in $AgNO_3$ solution. EDX spectra information along the length of Si pillars at different stages of processing. Digital photographs of load-bearing SiO_2 tube arrays (40 μm long) on water. This material is available free of charge via the Internet at http://pubs.acs.org.

■ AUTHOR INFORMATION

Corresponding Author

*D.-Y. Khang. E-Mail: dykhang@yonsei.ac.kr.

Notes

The authors declare no competing financial interest.

■ ACKNOWLEDGMENTS

This work was supported by the National Research Foundation Grant funded by the Korean Government (MEST) (NRF-2010-C1AAA001-0029061).

■ REFERENCES

(1) Nakamura, H.; Matsui, Y. *J. Am. Chem. Soc.* **1995**, *117*, 2651−2652.
(2) Mitchell, D. T.; Lee, S. B.; Trofin, L.; Li, N.; Nevanen, T. K.; Soderlund, H.; Martin, C. R. *J. Am. Chem. Soc.* **2002**, *124*, 11864−11865.
(3) Yang, X.; Tang, H.; Cao, K.; Song, H.; Sheng, W.; Wu, Q. *J. Mater. Chem.* **2011**, *21*, 6122−6135.
(4) Zhu, J.; Peng, H. L.; Conner, S. T.; Cui, Y. *Small* **2009**, *5*, 437−439.
(5) Kim, M.; Hong, J.; Lee, J.; Hong, C. K.; Shim, S. E. *J. Colloid Interface Sci.* **2008**, *322*, 321−326.
(6) Wang, F. K.; Li, D.; Mao, C. B. *Adv. Funct. Mater.* **2008**, *18*, 4007−4013.
(7) Adachi, M.; Harada, T.; Harada, M. *Langmuir* **1999**, *15*, 7097−7100.
(8) Gu, D.; Baumgart, H.; Abdel-Fattah, T. M.; Namkoong, G. *ACS Nano* **2010**, *4*, 753−758.
(9) Fan, R.; Wu, Y.; Li, D.; Yue, M.; Majumdar, A.; Yang, P. *J. Am. Chem. Soc.* **2003**, *125*, 5254−5255.
(10) Peng, K. Q.; Yan, Y. J.; Gao, S. P.; Zhu, J. *Adv. Mater.* **2002**, *14*, 1164−1167.
(11) Peng, K. Q.; Yan, Y. J.; Gao, S. P.; Zhu, J. *Adv. Funct. Mater.* **2003**, *13*, 127−132.
(12) Huang, Z.; Geyer, N.; Werner, P.; de Boor, J.; Gosele, U. *Adv. Mater.* **2011**, *23*, 285−308.
(13) Zhong, Z.; Yang, C.; Leiber, C.M. In *Nanosilicon*; Kumar, V., Ed.; Elsevier: New York, 2008; p 176.
(14) Balasundaram, K.; Sadhu, J. S.; Shin, J. C.; Azeredo, B.; Chanda, D.; Malik, M.; Hsu, K.; Rogers, J. A.; Ferreira, P.; Li, X. *Nanotechnology* **2012**, *23*, 305304.
(15) Mikhael, B.; Elise, B.; Xavier, M.; Sebastian, S.; Johann, M.; Laetitia, P. *ACS Appl. Mater. Interfaces* **2011**, *3*, 3866−3873.
(16) Qu, Y.; Zhou, H.; Duan, X. *Nanoscale* **2011**, *3*, 4060−4068.
(17) Li, X. *Curr. Opin. Solid State Mater. Sci.* **2012**, *16*, 71−81.
(18) Hochbaum, A. I.; Chen, R.; Delgado, R. D.; Liang, W.; Garnett, E. C.; Najarian, M.; Majumdar, A.; Yang, P. D. *Nature* **2008**, *451*, 163−167.
(19) Choi, J.-H.; Sung, J.; Moon, K.-j.; Jeon, J.; Kang, Y. H.; Lee, T. I.; Park, C.; Myoung, J.-M. *J. Mater. Chem.* **2011**, *21*, 13256−13261.
(20) Yoon, S.-S.; Khang, D.-Y. *Small* **2013**, *9*, 905−912.
(21) Kim, J.-H.; Hwang, H.-S.; Hahm, S.-W.; Khang, D.-Y. *Langmuir* **2010**, *26*, 13015−13019.
(22) Yoon, S.-S.; Khang, D.-Y. *J. Mater. Chem.* **2012**, *22*, 10625−10630.
(23) Hu, D. L.; Chan, B.; Bush, J. W. M. *Nature* **2003**, *424*, 663−666.

(24) Shi, F.; Niu, J.; Liu, J.; Liu, F.; Wang, Z.; Feng, X.-Q.; Zhang, X. *Adv. Mater.* **2007**, *19*, 2257−2261.
(25) Feng, X.-Q.; Gao, X.; Wu, Z.; Jiang, L.; Zheng, Q.-S. *Langmuir* **2007**, *23*, 4892−4896.
(26) Pan, Q.; Wang, M. *ACS Appl. Mater. Interfaces* **2009**, *1*, 420−423.
(27) Suzuki, K. In *Biomimetics Learning from Nature*; Mukherjee, A., Ed.; In-Tech: 2010.
(28) Pan, Q.; Liu, J.; Zhu, Q. *ACS Appl. Mater. Interfaces* **2010**, *2*, 2026−2030.
(29) Kim, J.; Han, H.; Kim, Y. H.; Choi, S.-H.; Kim, J.-C.; Lee, W. *ACS Nano* **2011**, *5*, 3222−3229.
(30) Lehmann, V. *Electrochemistry of Silicon: Instrumentation, Science, Materials and Applications*; Wiley-VCH: Weinheim, Germany, 2002; p 139.
(31) Peer, E.; Artzy-Schnirman, A.; Gepstein, L.; Sivan, U. *ACS Nano* **2012**, *6*, 4940−4946.
(32) Sze, S. M. *Semiconductor Devices: Physics and Technology*; John Wiley & Sons: New York, 2002; p 371.
(33) Schrtcliffe, N. J.; McHale, G.; Newton, M. I. *Appl. Phys. Lett.* **2006**, *89*, 104106.
(34) Dubash, N.; Frigaard, I. A. *J. Non-Newtonian Fluid Mech.* **2007**, *142*, 123−134.
(35) Dunkin, R. C.; McLellan, W. A.; Blum, J. E.; Ann Pabst, D. *Mar. Mammal Sci.* **2010**, *26*, 573−587.
(36) Chini, S. F.; Amirfazli, A. *Langmuir* **2010**, *26*, 13707−13714.
(37) Chandra, D.; Yang, S. *Acc. Chem. Res.* **2010**, *43*, 1080−1091.